

Thermodynamic instabilities in holographic neutron stars at finite temperature

Carlos R. Argüelles,^{a,b} Tobías Canavesi,^{a,c} Manuel Díaz,^c and Nicolás Grandi.^{c,b}

^a*Facultad de Ciencias Astronómicas y Geofísicas de La Plata,
Paseo del Bosque s/n, B1900FWA La Plata, Argentina*

^b*Departamento de Física, Universidad Nacional de La Plata,
Calle 49 y 115 s/n, CC67, 1900 La Plata, Argentina*

^c*Instituto de Física de La Plata,
Diagonal 113 e/63 y 64, CC67, 1900 La Plata, Argentina*

E-mail: charly@carina.fcaglp.unlp.edu.ar,
tcanavesi@fisica.unlp.edu.ar, mnig.diaz@gmail.com,
grandi@fisica.unlp.edu.ar

ABSTRACT: In a recent work we explored the backreaction of a self-gravitating system of elementary neutral fermions at finite temperature in asymptotically AdS space, known as the “holographic neutron star”. Such study was carried out by solving the Tolman-Oppenheimer-Volkoff equations under a perfect fluid assumption for the fermionic equation of state, accounting for both relativistic and finite temperature effects. Novel “dense core - diluted halo” density profiles in the AdS bulk were found, with corresponding two-point scalar field correlators obtained within the world line formalism, as a probe of the dual field theory. In this work we cover a much broader free parameter-space of the fermionic solutions in the bulk (from dilute to highly degenerate regime including for the critical point of gravitational collapse), and study their thermodynamic stability by calculating the grand canonical potential and free entropy. Such a stability analysis is performed using the Katz criterion, a technique historically applied to study the gravothermal catastrophe proper of classical self-gravitating systems in flat space. We identify some characteristic features of the unstable regions, both from the bulk and boundary perspectives, that can be used as proxies to detect instabilities on this kind of self-gravitating systems.

Contents

1	Introduction	2
2	The bulk perspective	3
2.1	Building the bulk state: a self-gravitating fluid at finite temperature	3
2.2	Probing the bulk state: scattering of a Euclidean massive particle	5
2.3	Results from the bulk perspective	7
3	The boundary perspective	11
3.1	Building the boundary state: grand canonical potential	11
3.2	Probing the boundary state: correlator of a scalar operator	13
3.3	Results from the boundary perspective	14
4	Bulk and boundary comparison	14
5	Discussion	19

1 Introduction

The thermodynamics of self gravitating systems is a fascinating subject with more than 50 years of related research [1–3]. The particularity introduced by the long range and unshielded nature of gravitational interaction is that equilibrium states become non-homogeneous, and the resulting thermodynamics is not extensive [3]. Indeed, due to the nonadditivity of the energy in systems with long range interactions, there is an inequivalence of ensembles in self-gravitating systems [1, 4], in contrast with the traditional thermodynamics of gases or plasmas. In particular, the thermodynamic properties of a self-gravitating neutral fermionic fluid, or “neutron star”, were first described in [5] within Newtonian gravity, and many years later within general relativity in [6]. The availability of more powerful numerical resources in recent years, allowed for a more detailed description of the different phases and their thermodynamic stability in different ensembles [3, 7, 8]. Regarding the dynamical equilibrium, the Tolman-Oppenheimer-Volkoff equations for a perfect fermionic fluid at finite temperature, present a rich set of solutions as a function of the central temperature and the central degeneracy [9]. Such states develop a “massive core - diluted halo” structure as the central degeneracy is increased at fixed central temperature, until the central core reaches the critical point of gravitational collapse [10].

These general relativistic studies have phenomenological as well as theoretical applications. From the phenomenological perspective, in [8] such fermionic mass distributions were used to model massive stars such as red giants or supernova with a possible subsequent collapse to a black hole in the latter. On the other hand in [11–17] the “core - halo” configurations were used to model dark matter halos in galaxies, providing rotation curves that are well fitted to observations, while the central core is able to mimic massive black hole at the galactic centers for KeV particle masses. From the theoretical side on the other hand, in [18] an AdS asymptotics was imposed, in order to interpret the system as a “holographic neutron star” dual to degenerate fermionic state of a conformal field theory defined on a sphere [19, 20], and scalar correlators were calculated.

In this work, we explore further the AdS construction, with emphasis on the thermodynamic stability of the fermion gas, using the rigorous stability criterion first developed by Katz [21] for classical self-gravitating systems in flat space. The main results presented on [18] were that (i) the core-halo profiles also show up in the AdS case, and (ii) the scalar correlators of the boundary theory develop a “swallow tale” structure as the central degeneracy is increased. Here, we explore further this system, with particular interest in its thermodynamics instabilities, both from the bulk and holographic perspective. Our main goal is to calculate the grand canonical potential and free entropy of the AdS solutions and to express it as a function of the boundary temperature and chemical potential - instead of the central quantities. Our main result is to identify characteristic features of the unstable regions, both from the bulk and boundary descriptions, that can be used as proxies to diagnose instability in this kind of systems. We demonstrate that the gravitational collapse occurs inside the unstable regions, indicating that the instabilities we found correspond to the confinement to deconfinement transition of the boundary theory.

2 The bulk perspective

From the bulk perspective, we will be interested in a neutron star solution in an asymptotically globally AdS spacetime, first studied in [19, 20].

2.1 Building the bulk state: a self-gravitating fluid at finite temperature

The model We want to describe the thermodynamics of a very large number of neutral self-gravitating fermions in equilibrium in $3 + 1$ dimensions in global AdS spacetime. We approximate the dynamics with a perfect fluid coupled to the gravitational field. We use the action

$$S = S_{\text{Gravity}} + S_{\text{Fluid}} . \quad (2.1)$$

Here the gravity part reads

$$S_{\text{Gravity}} = \frac{1}{16\pi G} \int d^4x \sqrt{-g} (R - 2\Lambda) , \quad (2.2)$$

where $\Lambda = -3/L^2$ being L the AdS length, and we chose natural units such that $\hbar = c = k_B = 1$ throughout this work. On the other hand the perfect fluid part can be written as a Schutz action

$$S_{\text{Fluid}} = \int d^4x \sqrt{-g} (-\rho + \sigma u^\mu (\partial_\mu \phi + \theta \partial_\mu s) + \lambda (u_\mu u^\mu + 1)) , \quad (2.3)$$

where ρ is the fluid energy density taken as a function of the fluid particle density σ and s the entropy per particle, while u_μ is its four-velocity. The variables ϕ , θ and λ are auxiliary Lagrange multipliers, enforcing that the particle number σ and the entropy density σs are conserved, and that the four-velocity u_μ is a time-like unit vector. The resulting equations of motion read

$$\sigma (\partial_\mu \phi + \theta \partial_\mu s) = -\lambda u_\mu , \quad (2.4)$$

$$u^\mu (\partial_\mu \phi + \theta \partial_\mu s) = \mu , \quad (2.5)$$

$$u_\mu u^\mu = -1 , \quad (2.6)$$

$$\partial_\mu (\sigma u^\mu) = 0 , \quad (2.7)$$

$$\partial_\mu (\sigma s u^\mu) = 0 , \quad (2.8)$$

$$u^\mu \partial_\mu \theta = -T , \quad (2.9)$$

$$G_{\mu\nu} + \Lambda g_{\mu\nu} = 8\pi G (P g_{\mu\nu} + (P + \rho) u_\mu u_\nu) . \quad (2.10)$$

In these equations we have defined the local chemical potential $\mu \equiv d\rho/d\sigma$, local temperature $\sigma T \equiv d\rho/ds$, and pressure $P \equiv -\rho + \mu\sigma$. The equations in the first two lines fix the auxiliary variables, implying $\lambda = \mu\sigma$ and $\partial_\mu \phi + \theta \partial_\mu s = -\mu u_\mu$. The third imposes that the four-velocity is unitary and time-like. The next two lines correspond to the conservation of the particle current σu^μ and the entropy current $\sigma s u^\mu$. Then we define the temperature as the proper time derivative of the “thermasy” θ . The last line contains the Einstein equations.

The above equations of motion need to be supplemented with an explicit dependence of ρ in σ and s . In the limit $mL \gg 1$, in which there is a large number of particles within one AdS radius [19], we can define such relation implicitly by

$$\rho = \frac{g}{8\pi^3} \int f(p) \sqrt{p^2 + m^2} d^3p, \quad (2.11)$$

$$P = \frac{g}{24\pi^3} \int f(p) \frac{p^2}{\sqrt{p^2 + m^2}} d^3p, \quad (2.12)$$

where g is the number of fermionic species or spin degeneracy, the integration runs over all momentum space, and $f(p)$ is the Fermi distribution for a fermion of mass m with local temperature T and local chemical potential μ

$$f(p) = \frac{1}{e^{\frac{\sqrt{p^2 + m^2} - \mu}{T}} + 1}. \quad (2.13)$$

The Ansatz We solved the above equations of motion with a stationary spherically symmetric “neutron star” Ansatz with the form

$$ds^2 = L^2(-e^{\nu(r)} dt^2 + e^{\lambda(r)} dr^2 + r^2 d\Omega_2^2), \quad (2.14)$$

$$u^\mu = u(r) \partial_t, \quad (2.15)$$

where $d\Omega_2^2 = d\vartheta^2 + \sin^2\vartheta d\varphi^2$ is a two-sphere. The local temperature T and chemical potential μ are then radial functions. Defining the functions \tilde{M} and χ by

$$e^\lambda = \left(1 - \frac{2\tilde{M}}{r} + r^2\right)^{-1}, \quad (2.16)$$

$$e^\nu = e^\chi \left(1 - \frac{2\tilde{M}}{r} + r^2\right), \quad (2.17)$$

equations (2.4)-(2.10) become the thermodynamic equilibrium conditions of Tolman and Klein

$$e^{\frac{\nu}{2}} \tilde{T} = \text{constant}, \quad (2.18)$$

$$e^{\frac{\nu}{2}} \tilde{\mu} = \text{constant}, \quad (2.19)$$

and the Einstein equations

$$\frac{d\tilde{M}}{dr} = 4\pi r^2 \tilde{\rho}, \quad (2.20)$$

$$\frac{d\chi}{dr} = 8\pi r \left(\tilde{P} + \tilde{\rho}\right) e^\lambda. \quad (2.21)$$

In the above expressions we have written the dimensionless combinations $\tilde{T} = T/m$ and $\tilde{\mu} = \mu/m$ for the temperature and chemical potential. The constants are obtained by evaluating the expression at a reference point, conventionally taken at $r = 0$. Moreover, we have re-scaled the density $\tilde{\rho} = GL^2 \rho$ and pressure $\tilde{P} = GL^2 P$. They are obtained

from (2.11) and (2.12) rewritten in terms of the variable $\epsilon = \sqrt{1 + p^2/m^2}$, resulting in the expressions

$$\tilde{\rho} = \gamma^2 \int_1^\infty \frac{\epsilon^2 \sqrt{\epsilon^2 - 1}}{e^{\frac{\epsilon - \tilde{\mu}}{T}} + 1} d\epsilon, \quad (2.22)$$

$$\tilde{P} = \frac{\gamma^2}{3} \int_1^\infty \frac{\left(\sqrt{\epsilon^2 - 1}\right)^3}{e^{\frac{\epsilon - \tilde{\mu}}{T}} + 1} d\epsilon, \quad (2.23)$$

where $\gamma^2 = gGL^2 m^4 / 2\pi^2$.

By expanding the equations (2.20) and (2.21) around the center of the configuration $r = 0$, we obtain the boundary conditions that correspond to a regular metric, as

$$\tilde{M}(0) = 0, \quad (2.24)$$

$$\chi(0) = 0, \quad (2.25)$$

$$\tilde{T}(0) = \tilde{T}_0, \quad (2.26)$$

$$\tilde{\mu}(0) = \mu_0 \equiv \Theta_0 \tilde{T}_0 + 1. \quad (2.27)$$

Here Θ_0 is called the “central degeneracy”, and we used it as a way to parameterize the central chemical potential. Families of solutions are then indexed by the parameters $(\tilde{T}_0, \Theta_0, \gamma^2)$.

2.2 Probing the bulk state: scattering of a Euclidean massive particle

In order to probe the resulting gravitational background, we study the scattering of a massive particle with an Euclidean worldline. The trajectories are obtained by extremizing the Euclidean particle action

$$S_{\text{Particle}}^E = m \int d\tau_E \sqrt{g_{\mu\nu} x'^\mu x'^\nu}. \quad (2.28)$$

Here m is the mass of the particle, $x^\mu(\tau_E)$ describes the geodesic in terms of an Euclidean parameter τ_E , and a prime ($'$) means a derivative with respect to τ_E . Evaluated on our Ansatz (2.14) this action reads

$$S_{\text{Particle}}^E = mL \int d\varphi \sqrt{r^2 + e^{\lambda(r)} r'^2}, \quad (2.29)$$

where we specialized to constant time $t' = 0$ and chose coordinates such that the trajectory lies in the equator of the sphere $\vartheta = \pi/2$. Moreover we fixed the reparametrization gauge as $\tau_E = \varphi$. The resulting system is invariant under shifts of the Euclidean parameter φ , resulting in a conserved quantity

$$r_* = \frac{r^2}{\sqrt{r^2 + e^{\lambda(r)} r'^2}}. \quad (2.30)$$

The value of r_* coincides with the value of the coordinate r at tip of the trajectory, defined as the point at which $r' = 0$. It can be used to label different geodesics by their minimum approach r_* to the center of the geometry.

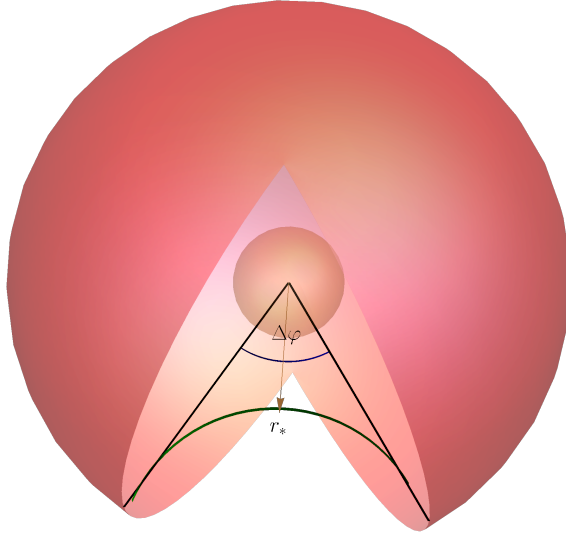


Figure 1. We study the scattering problem of a massive Euclidean particle entering the geometry from infinity, approaching the neutron star up to a tip radius r_* , and then moving again to the asymptotic region, spanning an angle $\Delta\varphi$.

We are interested in geodesics starting at a very large radius r_ϵ , falling into the geometry up to a minimum radius r_* , and then bouncing back into the asymptotic region, spanning a total angle $\Delta\varphi$ (see Fig.1). Then, our boundary conditions are

$$r|_{\varphi=0} = r|_{\varphi=\Delta\varphi} = r_\epsilon, \quad (2.31)$$

here $\Delta\varphi$ can be calculated according to

$$\Delta\varphi = \int d\varphi = \int \frac{dr}{r'}. \quad (2.32)$$

Solving (2.30) for the velocity r' and using the fact that the trajectory is symmetric around its tip, we get $\Delta\varphi$ as a function of r_* , in the form

$$\Delta\varphi = 2r_* \int_{r_*}^{r_\epsilon} dr \frac{e^{\frac{\lambda(r)}{2}}}{r\sqrt{r^2 - r_*^2}}. \quad (2.33)$$

For $r_* = 0$ we have no scattering and then $\Delta\varphi = \pi$. On the other hand in the limit of very large r_* we get $\Delta\varphi = 0$, implying a backward scattering. In the intermediate region, the behaviour of $\Delta\varphi$ can be either monotonic or non-monotonic. In the last case, the same angle $\Delta\varphi$ is spanned by geodesics with different values of the minimum approach radius r_* .

Due to the symmetries of the problem, a value of $\Delta\varphi$ larger than π is not physically different from the value smaller than π obtained by the transformation $\Delta\varphi \rightarrow 2\pi - \Delta\varphi$. This is evident in Fig.1. Thus, in what follows we restrict $\Delta\varphi$ to values smaller than π , applying such transformation whenever the integral (2.33) returns a value larger than π . This may result in a non-monotonic behaviour of $\Delta\varphi$ as a function of r_* , see Fig.2.

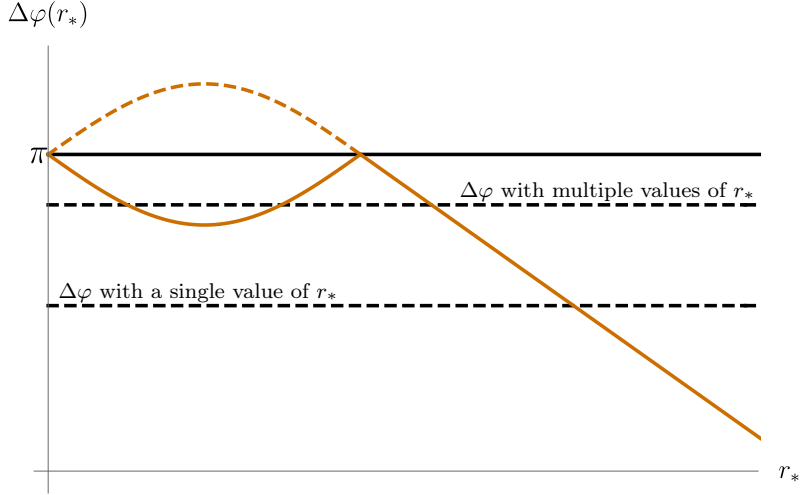


Figure 2. The angle $\Delta\varphi$ as a function of the tip position r_* . Whenever the integral (2.33) returns a value larger than π (dotted curve), it must be mapped to $2\pi - \Delta\varphi$ (continuous curve). Notice that this results in a non-monotonic behaviour, with three different values of r_* returning the same value of $\Delta\varphi$, for $\Delta\varphi$ close enough to π .

2.3 Results from the bulk perspective

We solved the above system of equations (2.18)-(2.23) with boundary conditions (2.24)-(2.27) numerically using a **Mathematica** routine. We explored the (\tilde{T}_0, Θ_0) plane for a fixed value of γ^2 . At each point, we evaluated the function (2.33) determining whether the angle $\Delta\varphi$ is a monotonic function of r_* . The results are shown in Figs. 3 and 4.

At positive enough central degeneracy $\Theta_0 \gtrsim 10$ and sufficiently small central temperature \tilde{T}_0 , the density profiles have a well defined core-halo structure as exemplified in Fig. 3, in complete analogy with the asymptotically flat space [11, 15]. For such range of parameters, the highly-dense core is supported by degeneracy pressure while the outer halo (or diluted atmosphere) is hold against gravity by thermal pressure. The halo ends at a sharp edge at which the boundary of the star is reached, thanks to the overall AdS inward-pressure term. As the central temperature is increased at fixed central degeneracy, the compacity of the central core increases, until the critical temperature of gravitational collapse is reached \tilde{T}_0^{cr} . Interestingly, above such critical value, *e.g.* $\tilde{T}_0^{cr} \approx 10^{-2}$ for $\Theta_0 = 30$, the outer halo region (just before the sharp edge) as well as the inner dense-core develop a power law morphology analogously as found in the asymptotically flat case [9]. The critical point of gravitational collapse to a singularity is evidenced with the presence of a local maximum of the total mass as a function of the central density (see the examples of $\Theta_0 = 30, 50$ in Fig. 3). Its existence is typical of any relativistic self-gravitating system of fermions, as shown in [20] within the fully degenerate limit ($\tilde{T} \rightarrow 0$) in AdS, and in [10] or [18] for the more general finite-temperature cases either in flat space, or AdS respectively. Remarkably, by increasing further the central temperature, a non-monotonic behaviour on the Euclidean geodesics appears (see Fig. 3). This result was not known from the recent related work [18] by the authors, since only $\tilde{T}_0 \lesssim \tilde{T}_0^{cr}$ values were explored.

At negative central degeneracy $\Theta_0 < 0$, the fermions are in the Boltzmannian regime of the Fermi-Dirac distribution, thus the star is fully supported by thermal pressure (for fixed AdS length). In this case the profiles have no core, but just an overall diluted density profile with an inner constant value followed by a smooth transition towards the sharp edge, for small enough central temperature \tilde{T}_0 , see Fig. 4. As the central temperature is increased, the star gets more extended and massive, with an outer region, just before the sharp edge, developing a power law trend with a mild (non degeneracy-supported) core at the center. Such morphological density profile behaviour resembles somehow the $\Theta_0 > 10$ case, and imply a non-monotonic trend of the geodesics. At some point \tilde{T}_0 would reach the critical temperature for gravitational collapse, though such value is above our maximum parameter-space coverage *e.g.* $\tilde{T}_0 < 10^{-1}$, and certainly close to the ultra relativistic regime $\tilde{T}_0 \sim 1$. Consequently, in the total mass *vs.* central density plots the maximum is not reached, see Fig. 4.

These results can be summarized in a phase diagram as shown in Fig. 5. The power law behaviour at the boundary of the density profile, as well as the non-monotonic behaviour on the geodesics, appear at intermediate degeneracies and high enough temperatures. Remarkably, this can be linked with the boundary perspective physics, as explicated in section 3 below.

The fact that \tilde{T}_0^{cr} is considerably larger for negative to small central degeneracies respect to the $\Theta_0 > 10$ case discussed above, is understood in terms of the maximum possible pressure holding the star against gravity. While in the first scenario the fermions needs to be close to the ultra-relativistic regime for the thermal pressure to acquire its maximum value, in the later, is the fully degeneracy limit, given by $\Theta_0 \gg 1$ for low enough \tilde{T}_0 , the one halting gravity before the collapse. Moreover, it can be shown that while the critical mass for collapse is $\text{Log} \tilde{M}^{cr} \approx -6$ in the highly degenerate cases, see Fig. 3, it starts to grow above this value for lower and lower Θ_0 showing the temperature effects, in complete analogy to asymptotically flat case [10]. Finally, for positive and small central degeneracies $0 \lesssim \Theta_0 \lesssim 10$, the fermions are in a semi-degenerate regime developing a mild core - diluted halo behaviour, though the core does not fulfill the quantum degeneracy condition $\lambda_B > 3l$, with λ_B the thermal de-Broglie wavelength and l the interparticle mean distance, as first demonstrated in [11] in flat space.

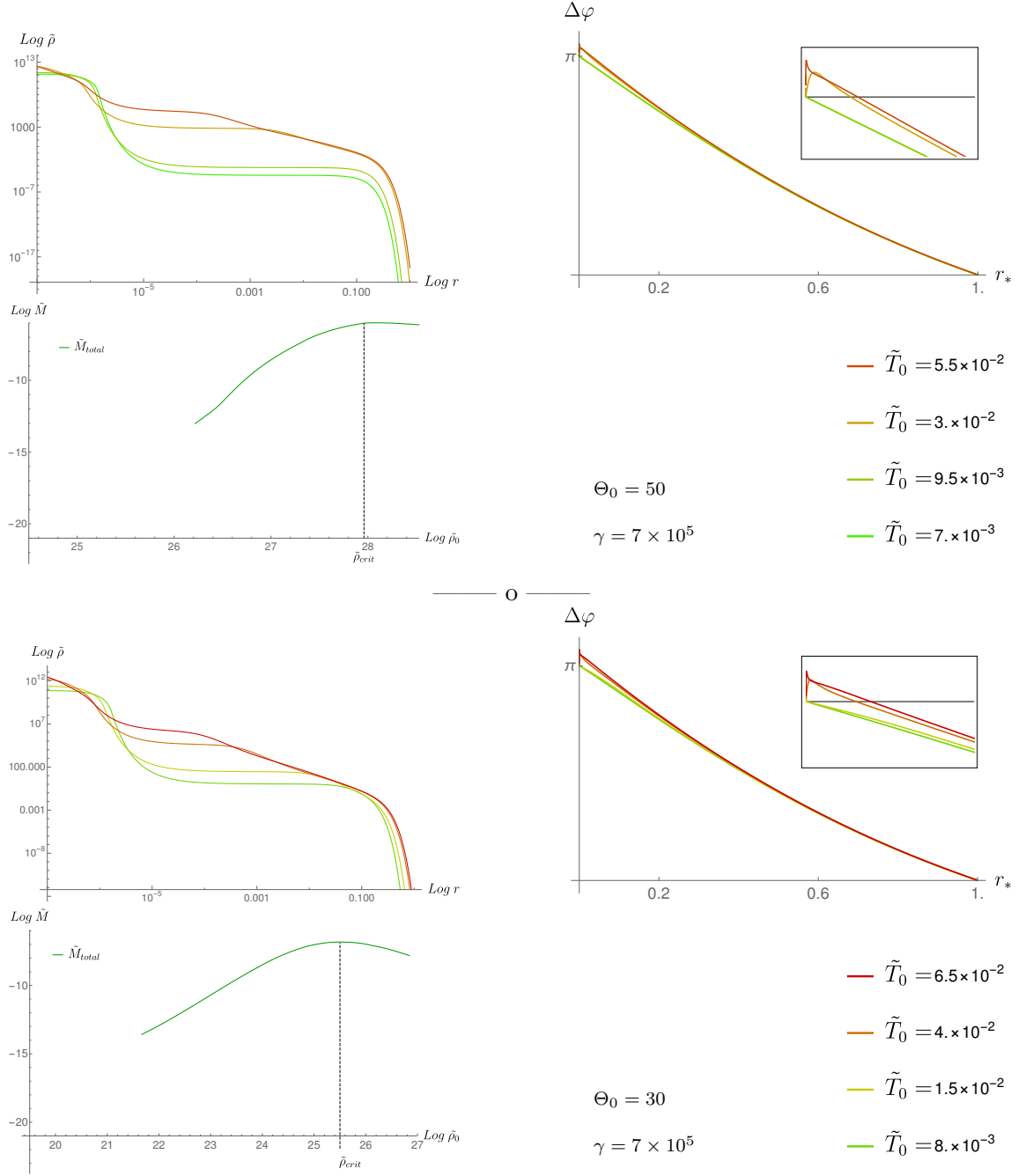


Figure 3. Plots of the solutions corresponding to $\Theta_0 = 50$ (first set of three plots) and $\Theta_0 = 30$ (second set of three plots) for different values of \tilde{T}_0 . Up-left: logarithmic plot of the density profile as a function of the radius. The density has a dense core and a diluted halo that decreases sharply at the boundary of the star for low temperatures, while for $\tilde{T}_0 > \tilde{T}_0^{cr}$ it takes a power law form. Up-right: the angle $\Delta\varphi$ between the incident and scattered direction of a massive Euclidean geodesic. For the profiles with a power law decay, it grows into values bigger than π , as can be seen in the inset. Down-left: the total mass M as a function of the central density. We see that there is a local maximum at the temperatures at which the power law behaviour shows up.

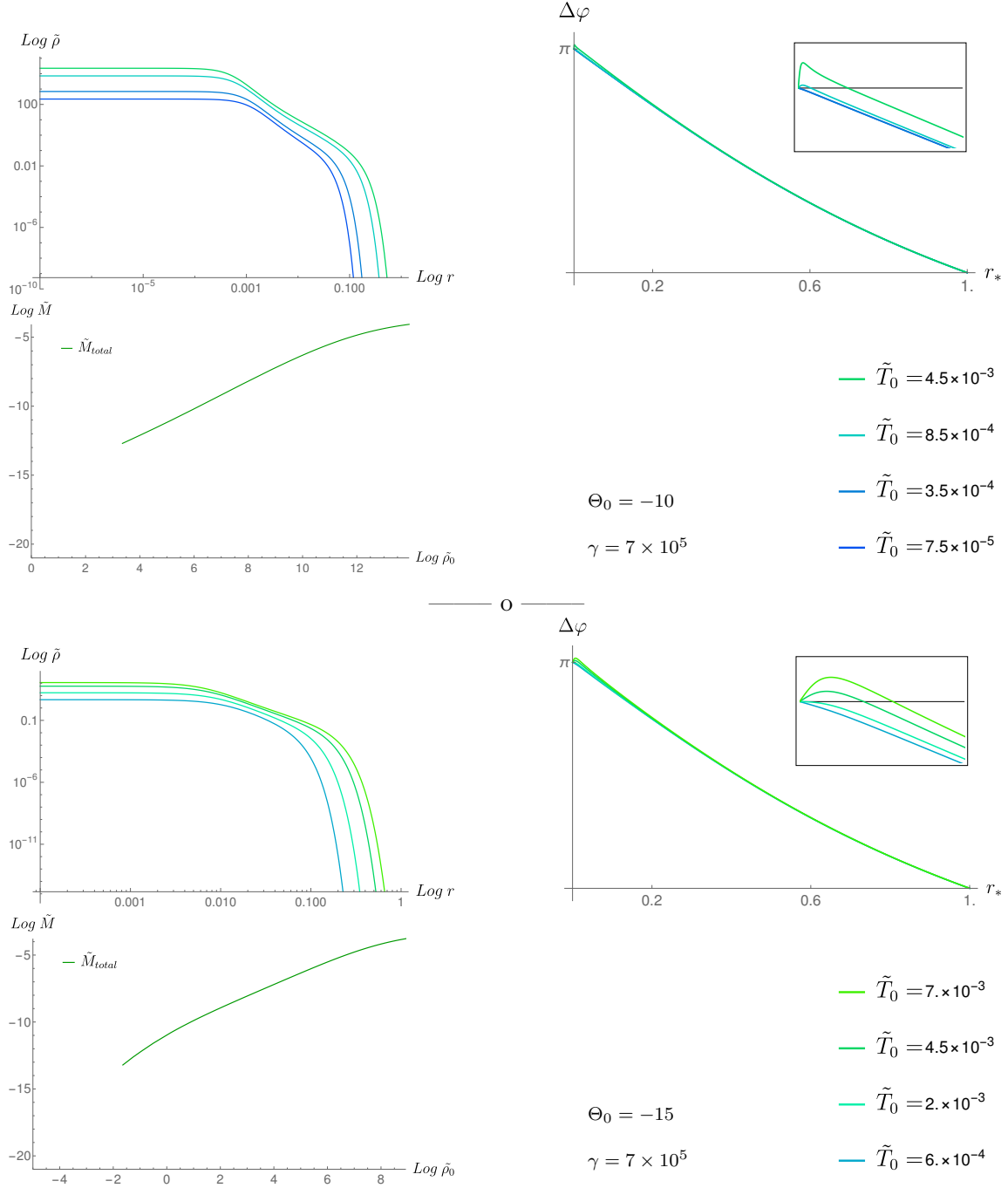


Figure 4. Plots of the solutions corresponding to $\Theta_0 = -10$ (first set of three plots) and $\Theta_0 = -15$ (second set of three plots) for different values of \tilde{T}_0 . Up-left: logarithmic plot of the density profile as a function of the radius. The density has a plateau and decreases sharply at the boundary of the star for low temperatures, while for higher temperatures it takes a power law form. Up-right: the angle $\Delta\varphi$ between the incident and scattered direction of a massive Euclidean geodesic. For the profiles with a power law decay, it grows into values bigger than π . Down-left: the total mass M as a function of the central density. We see that there is no special feature at the temperatures at which the power law behaviour shows up.

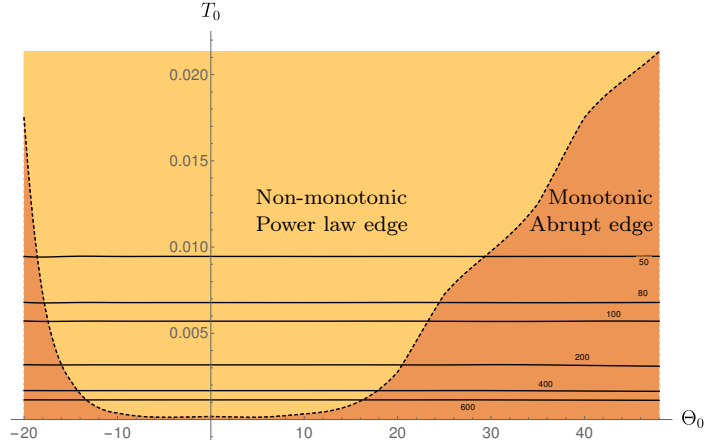


Figure 5. Central temperature \tilde{T}_0 vs. central degeneracy Θ_0 phase diagram. In the yellow region the geodesics behave non-monotonically and the profiles have a power law edge. The horizontal lines are the level curves of the asymptotic quotient $\tilde{\mu}/\tilde{T}$, see below.

3 The boundary perspective

From the boundary point of view, the system under study corresponds to a highly degenerate fermionic state on a conformal field theory defined on a sphere, at finite temperature and chemical potential [19].

3.1 Building the boundary state: grand canonical potential

The on shell action: The grand canonical potential $\Omega(\mu, T)$ is calculated according to

$$\Omega(\tilde{\mu}, \tilde{T}) = m\tilde{T} S_{\text{on-shell}}^E, \quad (3.1)$$

where \tilde{T} and $\tilde{\mu}$ are the dimensionless boundary temperature and chemical potential respectively, obtained as the asymptotic values of the corresponding bulk functions. The magnitude $S_{\text{on-shell}}^E$ is the Euclidean action obtained by a Wick rotation $t_E = it$ of the action (2.1), supplemented with the Gibbons-Hawking-York term and the necessary holographic renormalization counterterms

$$S_{\text{on-shell}}^E = (S_{\text{Gravity}}^E + S_{\text{Fluid}}^E + S_{\text{GHY}}^E + S_{\text{ct}}^E)|_{\text{on-shell}}. \quad (3.2)$$

By evaluating these terms on the solution, we get

$$\Omega(\tilde{\mu}, \tilde{T}) = \frac{L}{G} e^{-\frac{\nu_\infty}{2}} \left(\tilde{M} - 4\pi \int dr e^{\frac{\nu+\lambda}{2}} r^2 (\tilde{\rho} + \tilde{P}) \right), \quad (3.3)$$

where \tilde{M} and ν_∞ correspond to the asymptotic value of the $\tilde{M}(r)$ and $\nu(r)$ respectively.

The on shell action is a natural function of the central parameters \tilde{T}_0 and Θ_0 . Since we are interested in the boundary physics, we want to write it as a parametric function of the boundary quantities \tilde{T} and $\tilde{\mu}$, which depend on \tilde{T}_0 and $\tilde{\mu}_0$ according to (2.18) and (2.19). Since the dependence is parametric, there is a chance that $\Omega(\tilde{T}, \tilde{\mu})$ is not singled valued. This situation is somewhat frequent in self gravitating systems, and we will discuss the issue in more detail below.

Stability analysis: Since the grand canonical potential might be multivalued, we need an criterion to determine which of its many branches corresponds to a stable phase of the boundary theory at a given temperature \tilde{T} and chemical potential $\tilde{\mu}$. We use the Katz stability criterion, that we sketch below.

We start with the entropy S and define the grand canonical free entropy as

$$\Phi(\tilde{T}, \tilde{\mu}) = S - \frac{1}{\tilde{T}} \tilde{M} - \frac{\tilde{\mu}}{\tilde{T}} N = -\frac{\Omega}{\tilde{T}}, \quad (3.4)$$

such that its derivative with respect to $1/\tilde{T}$ gives minus the mass $-\tilde{M}$ of the configuration. Next we assume that $\Phi(\tilde{T}, \tilde{\mu})$ can be extended away from the equilibrium configuration into a function $\Phi^{\text{ext}}(q_i, \tilde{T}, \tilde{\mu})$ that depends on the generalized coordinates q_i that parameterize the deviation from equilibrium. The equilibrium states are stationary points of the extended grand canonical free entropy Φ^{ext} .

$$\partial_i \Phi^{\text{ext}}(q_i, \tilde{T}, \tilde{\mu}) = 0. \quad (3.5)$$

We can write the equilibrium solutions of this equation as $q_i = q_i(\tilde{T}, \tilde{\mu})$, and recover the equilibrium grand canonical free entropy as

$$\Phi(\tilde{T}, \tilde{\mu}) = \Phi^{\text{ext}}(q_i(\tilde{T}, \tilde{\mu}), \tilde{T}, \tilde{\mu}). \quad (3.6)$$

Since the derivative of $\Phi(\tilde{T}, \tilde{\mu})$ with respect to the inverse temperature $1/\tilde{T}$ at fixed $\tilde{\mu}/\tilde{T}$ gives minus the mass $-\tilde{M}$, we can define an extended mass function as $-\tilde{M}^{\text{ext}} = \partial_{1/\tilde{T}} \Phi^{\text{ext}}(q_i, \tilde{T}, \tilde{\mu})$. Using (3.5) and (3.6) we can show that the equilibrium mass reads

$$-\tilde{M}(\tilde{T}, \tilde{\mu}) = -\tilde{M}^{\text{ext}}(q_i(\tilde{T}, \tilde{\mu}), \tilde{T}, \tilde{\mu}). \quad (3.7)$$

A derivative of this equation then gives

$$-\partial_{1/\tilde{T}} \tilde{M} = -\partial_{1/\tilde{T}} \tilde{M}^{\text{ext}} - \sum_i \partial_i \tilde{M}^{\text{ext}} \partial_{1/\tilde{T}} q_i. \quad (3.8)$$

The second term can be rearranged using the implicit function theorem in (3.5), to get

$$-\partial_{1/\tilde{T}} \tilde{M} = -\partial_{1/\tilde{T}} \tilde{M}^{\text{ext}} - \sum_{ij} \partial_i \tilde{M}^{\text{ext}} (\partial_i \partial_j \Phi^{\text{ext}})^{-1} \partial_j \tilde{M}^{\text{ext}}. \quad (3.9)$$

We can parameterize the deformation away from equilibrium with coordinates q_i such that the matrix $\partial_i \partial_j \Phi^{\text{ext}}$ is diagonal, as

$$-\partial_{1/\tilde{T}} \tilde{M} = -\partial_{1/\tilde{T}} \tilde{M}^{\text{ext}} - \sum_i \frac{(\partial_i \tilde{M}^{\text{ext}})^2}{\lambda_i}. \quad (3.10)$$

where q_i is now the direction in the deformation space characterized by the eigenvalue λ_i of the matrix $\partial_i \partial_j \Phi^{\text{ext}}$. When any of such eigenvalues, say λ , is close enough to zero, it dominates the right hand side of equation (3.10), resulting in

$$-\partial_{1/\tilde{T}} \tilde{M} \approx -\frac{(\partial_q \tilde{M}^{\text{ext}})^2}{\lambda}, \quad (3.11)$$

The crucial observation is that the sign of the eigenvalue is opposite to the sign of the expression $-\partial_{1/\tilde{T}}\tilde{M}$. Since this is valid whenever λ is approaching zero, the derivative is diverging at such points. In conclusion, whenever the plot of $-\tilde{M}$ versus $1/\tilde{T}$ at constant $\tilde{\mu}/\tilde{T}$ has a vertical asymptota, the slope of the curve at each side of the asymptota is opposite to the sign of the eigenvalue of $\partial_i\partial_j\Phi^{\text{ext}}$ that is approaching zero at that temperature.

In a stable or meta-stable equilibrium state, the grand canonical free entropy Φ^{ext} is a maximum. This implies that all the eigenvalues of $\partial_i\partial_j\Phi^{\text{ext}}$ are negative. As we move the inverse temperature at fixed $\tilde{\mu}/\tilde{T}$, the system evolves and the plot $-\tilde{M}$ versus $1/\tilde{T}$ eventually reaches a vertical asymptota. Since all the eigenvalues are negative, it approaches it with a positive slope. If at the other side of the asymptota the slope becomes negative, this implies that the one of the eigenvalues changed its sign, and the system reached an unstable region.

In what follows we identify the stable equilibrium state in which all the eigenvalues are negative with the diluted configurations, for which the central degeneracy Θ_0 is negative. Next, we follow the $-\tilde{M}$ versus $1/\tilde{T}$ curve until we reach an asymptota at which the slope changes its sign. For each change from positive to negative slope, we count a new positive eigenvalue. For each change from negative to positive slope, we count a new negative eigenvalue. Any region with at least one positive eigenvalue, is unstable.

3.2 Probing the boundary state: correlator of a scalar operator

In order to probe the field theory on the boundary, we consider a scalar operator, and we used the dictionary of the AdS/CFT correspondence to evaluate its two-point correlator. We consider two points in the boundary sphere, separated by an angle $\Delta\varphi$ at fixed Euclidean time. In the limit of a large conformal dimension $\Delta \equiv \mathfrak{m}L$, the correlator is given as

$$\langle\mathcal{O}(\Delta\varphi)\mathcal{O}(0)\rangle = \lim_{r_\epsilon\rightarrow\infty} r_\epsilon^{2\mathfrak{m}L} e^{-S_{\text{Particle}}^{E \text{ on-shell}}(\Delta\varphi)}, \quad (3.12)$$

where the exponent is the Euclidean particle action (2.28) evaluated on shell, and r_ϵ is an UV bulk regulator, whose power is included in the prefactor in order to get a finite result. Solving (2.30) for r' and plugging back into (2.29), we obtain the Euclidean action as

$$S_{\text{Particle}}^{E \text{ on-shell}} = 2\mathfrak{m}L \int_{r_*}^{r_\epsilon} dr \frac{r e^{\frac{\lambda(r)}{2}}}{r \sqrt{r^2 - r_*^2}}, \quad (3.13)$$

where we have included the same cutoff r_ϵ .

Equation (3.13) gives the on-shell action as a function of the position of tip if the geodesic r_* . Equation (2.33) on the other hand, provide $\Delta\varphi$ as a function of the same variable. This allows us to parametrically plot the the on-shell action as a function of the angular separation. Interestingly, for the cases in which $\Delta\varphi$ is non-monotonic as a function of r_* that we studied in section 2.2, there are three values of $S_{\text{Particle}}^{E \text{ on-shell}}$ for a single value of $\Delta\varphi$, *i.e.* the Euclidean particle action become multivalued. The correlator is then given by the absolute minimum of the Euclidean particle action, which corresponds to the smaller branch of the multivalued function.

3.3 Results from the boundary perspective

We calculated the grand canonical free entropy $\Phi(\tilde{T}, \tilde{\mu})$ for our numerical solutions, as well as their total mass $\tilde{M}(\tilde{T}, \tilde{\mu})$. The resulting curves are shown in Figs. 6 and 7, where we plot both magnitudes as functions of the inverse temperature at fixed $\tilde{\mu}/\tilde{T}$. They are multivalued functions as expected from their parametric definition. Starting from the most negative value of Θ_0 , identified as the stable branch, the curves of $-\tilde{M}$ vs. $1/\tilde{T}$ spirals into a succession of vertical asymptote in which the slope changes from positive to negative. This indicates that a succession of eigenvalues are becoming positive, increasing the degree of instability. At a certain point the process reverses, and the curve spirals out. Nevertheless the number of eigenvalues that change back to negative sign is not enough to restore local stability. At larger Θ_0 the curve spirals again into the gravitational collapse. Thus from the boundary perspective, the instability can be identified as the onset of the confinement to deconfinement transition [19, 20].

We also evaluated the two-point correlator (3.12) for the different backgrounds. This is depicted on the left hand side of Fig. 8. As the boundary temperature is increased, the Euclidean particle action becomes multivalued, developing a swallow tale form. Since the scalar correlator is given by its smaller branch, as can be seen in the figures it develops a non-vanishing angular derivative at zero angular separation. In Fig. 6 the branches of the free entropy at which the correlator is multivalued are identified with a dotted line. Interestingly, the swallow tale always appear after the first eigenvalue has become positive, *i.e.* inside an unstable branch of the free entropy plot.

4 Bulk and boundary comparison

In Figs. 6 and 7 we plot the thermodynamic curves corresponding to the grand canonical free entropy $\Phi = -\Omega/T$ and minus the mass $-\tilde{M}$, as functions of $1/\tilde{T}$ at fixed $\tilde{\mu}/\tilde{T}$. The central degeneracy Θ_0 plays the role of a parameter. Using the Katz stability criterion, we can differentiate between thermodynamically stable and thermodynamically unstable branches.

As main outcomes of such an analysis we conclude: (i) the stable to unstable transition always occur within the diluted fermionic regime, *i.e.* for $\Theta_0 \approx -20$ for all the values of $\tilde{\mu}/\tilde{T}$ here analyzed, and for \tilde{T}_0 well below the critical value; (ii) For somewhat larger negative Θ_0 , well inside the unstable branch at about the second vertical asymptote before the spiraling, the swallow tail behaviour in the correlator arises, coinciding with the non-monotonic to monotonic transition in $\Delta\varphi$ (see the phase-space diagram in Fig. 5 for comparison); (iii) Interestingly, the point in which the spiral starts to unwind in the $-\tilde{M}$ vs. $1/\tilde{T}$ plot, always within the unstable region, corresponds to the transition from diluted $\Theta_0 < 0$ to semi-degenerate $\Theta_0 > 0$ regime, in total analogy with the flat space case [22]; (iv) Already in the degenerate regime $\Theta_0 > 10$, and for $\tilde{T}_0 < \tilde{T}_0^{cr}$ (at about the second asymptote after unwinding), the swallow tail pattern in the correlator ends and so the non-monotonic trend in $\Delta\varphi$. The curves continue towards larger $\Theta_0 \gg 1$, until the critical point of collapse arises (*e.g.* for $\Theta_0 = 48$ and $\tilde{T}_0^{cr} = 2.1 \times 10^{-2}$ for $\tilde{\mu}/\tilde{T} = 80$). Such point corresponds to a *second* spiraling in the $-\tilde{M}$ vs. $1/\tilde{T}$ curve, as a manifestation of the gravitational collapse,

only evidenced here for $\tilde{\mu}/\tilde{T} = 50$ and $\tilde{\mu}/\tilde{T} = 80$ due to limitations in the space-parameter coverage, again resembling the flat space case [22].

In Fig. 8 the correlator as a function of the angular span $\Delta\varphi$ is compared with the angular span as a function of the minimum approach r_* . As expected, when $\Delta\varphi$ is non-monotonic as a function r_* , the corresponding Euclidean particle action is multivalued, and the resulting correlator has a non-vanishing derivative at zero angular separation.

In the section 2, we observed that density profiles with a power law edge appear in regions of parameters in which the angular span as a function of the tip position is non-monotonic see Fig. 5. Combined with the observation above, this implies that such power law edges show up only inside the unstable branches of the free entropy, denoted with a dotted line in Figs. 6 and 7.

Moreover, the features mentioned above appear together with the maximum of the mass as a function of the central density, which according to the turning point criterion signals the gravitational instability. This is another indication that the instability we are finding can be identified with the onset of the gravitational collapse occurring prior to the turning point, and corresponding to the confinement to deconfinement transition of the boundary theory. Our finite temperature analysis generalizes the results of [19, 20] in which the transition occurs precisely at the turning point.

The above suggest that, from the bulk perspective, a non-monotonic scattering problem or a power law edge in the density profile, are signals of a possible instability of the system. From the boundary perspective on the other hand, such role is played by a scalar correlator whose angular derivative does not vanish at zero angular separation.

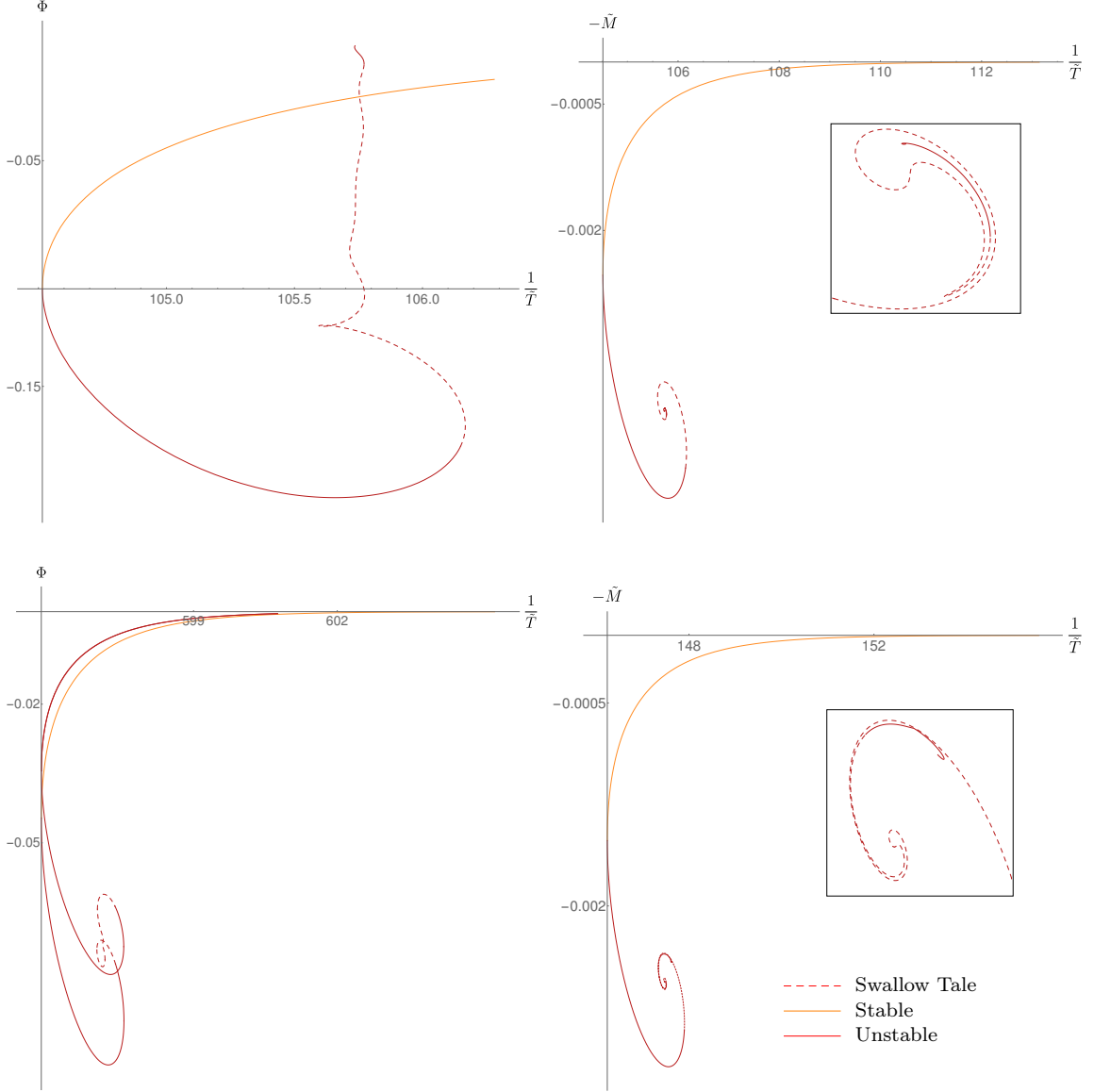


Figure 6. Parametric plot of the grand canonical free entropy Φ (left) and minus the total mass $-\tilde{M}$ (right) as functions of the inverse boundary temperature $1/\tilde{T}$, for a fixed value of $\mu/\tilde{T} = 50$ (first line) and $\mu/\tilde{T} = 80$ (second line). The curve starts at negative values of Θ_0 where all the eigenvalues are assumed to be negative (orange line). As the plot on right hand side reaches its first vertical asymptota, an eigenvalue changes sign from negative to positive (red line). The process repeats on each vertical asymptota in which the slope changes from positive to negative. At the center of the spiral (see inset) the process reverses and the slope starts to change from negative to positive at each vertical asymptota, the eigenvalues changing from positive into negative again. Nevertheless, the stability is not recovered an the system spirals back into the gravitational collapse. The dashed line corresponds to the region of parameters for which there is a swallow tale on the scalar correlators. We see that such behaviour always appear after $-\tilde{M}$ had reached its first vertical asymptota, *i.e.* in the unstable region.

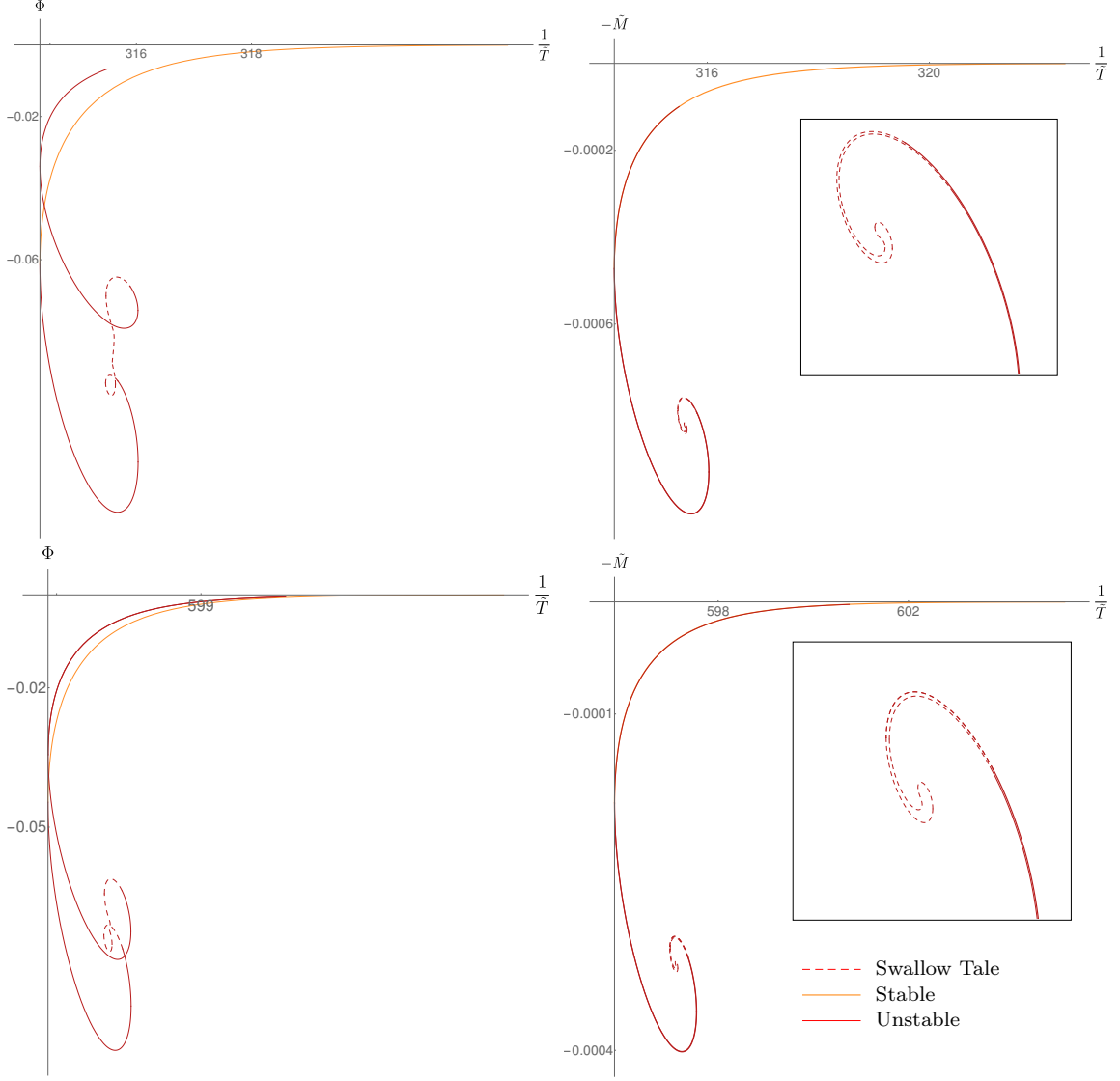


Figure 7. Parametric plot of the grand canonical free entropy Φ (left) and minus the total mass $-\tilde{M}$ (right) as functions of the inverse boundary temperature $1/\tilde{T}$, for a fixed value of $\mu/\tilde{T} = 200$ (first line) and $\mu/\tilde{T} = 400$ (second line). The curve starts at negative values of Θ_0 where all the eigenvalues are assumed to be negative (orange line). As the plot on right hand side reaches its first vertical asymptota, an eigenvalue changes sign from negative to positive (red line). The process repeats on each vertical asymptota in which the slope changes from positive to negative. At the center of the spiral (see inset) the process reverses and the slope starts to change from negative to positive at each vertical asymptota, the eigenvalues changing from positive into negative again. Nevertheless, there is always one eigenvalue remaining positive. The dashed line corresponds to the region of parameters for which there is a swallow tale on the scalar correlators. We see that such behaviour always appear after $-\tilde{M}$ had reached its first vertical asymptota, *i.e.* in the unstable region.

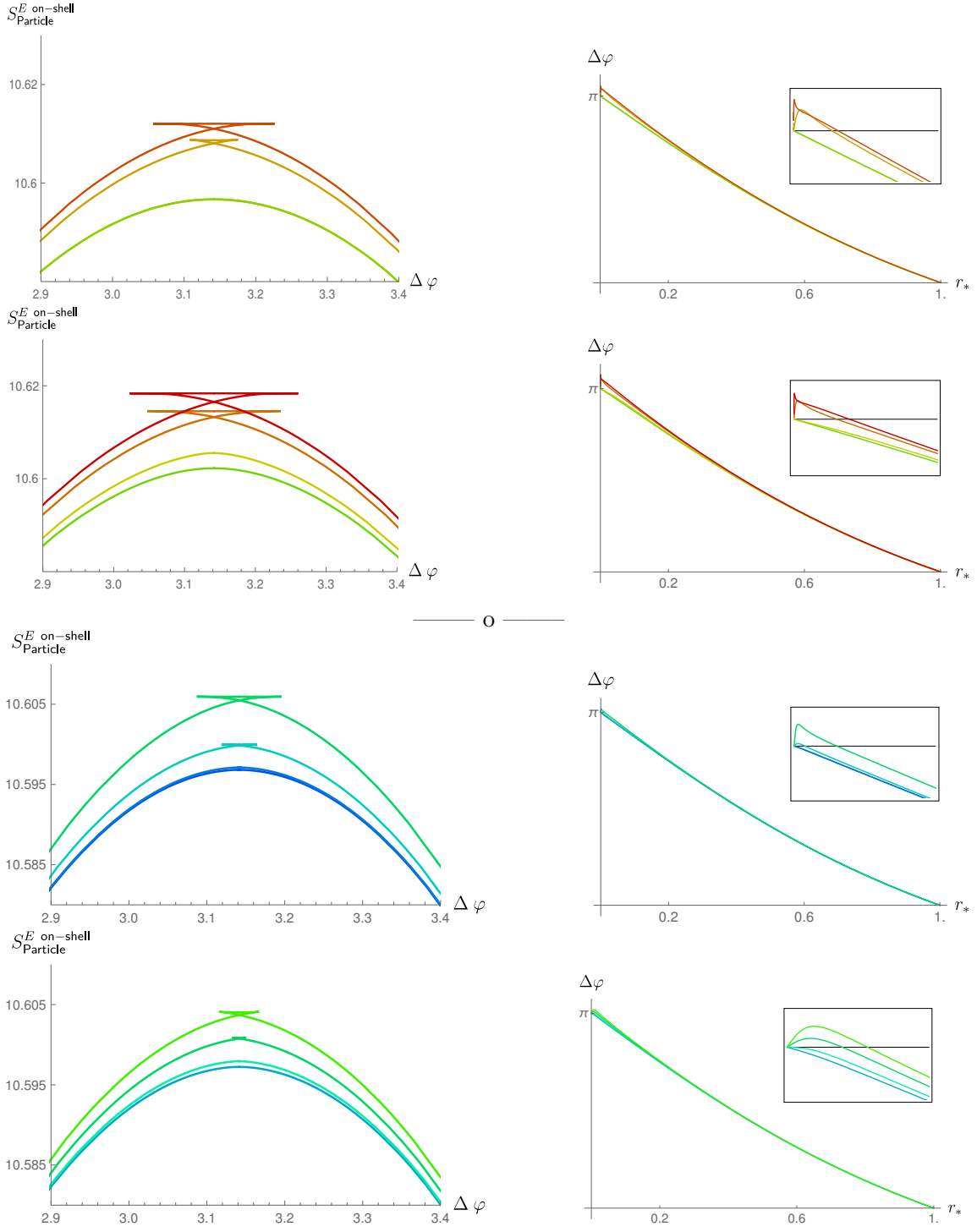


Figure 8. Plots corresponding to $\Theta_0 = 50$ and $\Theta_0 = 30$ (first two lines) and to $\Theta_0 = -10$ and $\Theta_0 = -15$ (third and fourth lines). Left: the on-shell Euclidean particle action as a function of the angular span $\Delta\varphi$ (the angular domain has been extended into negative values in order to get a clearer view); a swallow tale structure appears as the central temperature is increased. The scalar correlator corresponds to the smaller branch of such multivalued function, implying that it has a non-vanishing derivative at zero angular separation. Right: the angular span as a function of the geodesic tip r_* ; the non-monotonicity is what originates to the swallow tale on the left. Colors are correlated with Figs. 3 and 4.

5 Discussion

We studied the equilibrium states of a holographic neutron star from both the bulk and the boundary perspectives.

From the AdS bulk perspective, density profiles manifest a rich core - halo structure that was previously reported [18] and that is well understood in the asymptotically flat case [16]. A dense core and diluted halo are present at large central degeneracies Θ_0 , and disappear as the central degeneracy becomes negative. As the central temperature T_0 is increased, the initially sharp end of the star density profile as a function of the radius degenerates into a power law. This coincides with a maximum on the total mass \tilde{M} as a function of the central density. We probed the background with the scattering of a massive Euclidean particle, obtaining the spanned angle $\Delta\varphi$ as a function of the minimum radius r_* reached by the particle trajectory. We observed that, at the region of parameters where the density profile has a power law edge, this function is non-monotonic.

From the boundary perspective, we calculated the grand canonical free entropy and perform a Katz equilibrium analysis. We found that the system has a stable branch that destabilizes at a certain temperature and never stabilizes again. We calculated the holographic two point correlator of a scalar operator in the large conformal dimension limit, and verify that the non-monotonicity of the scattering problem gives rise to a correlator with a non-vanishing angular derivative at zero angular separation. Interestingly, such behaviour manifests only inside the unstable branches. Moreover, inside such branches we also observed bulk profiles with a power law edge.

As a main conclusion of the present work, the presence of a power law edge in the density profile, or of a non-monotonic scattering problem, can be taken as a signature of an unstable background from the bulk perspective. Conversely, from the boundary point of view, a correlator with a non-vanishing derivative at zero angular separation, is an indicator of a possible phase transition. Since after the onset of the instability the system goes into the gravitational collapse, we identify such phase transition as the confinement to deconfinement one, generalizing to finite temperature the results of [19, 20].

Acknowledgments

The authors thank Guillermo Silva, Diego Correa and Pablo Pisani for useful comments. This work has been funded by the CONICET grants PIP-2017-1109 and PUE 084 “Búsqueda de Nueva Física” and UNLP grant PID-X791.

References

- [1] T. Padmanabhan, “Statistical mechanics of gravitating systems,” *Physics Reports*, vol. 188, pp. 285–362, Apr. 1990.
- [2] J. Katz, “Thermodynamics and selfgravitating systems,” *Foundations of Physics*, vol. 33, no. 2, pp. 223–269, 2003.
- [3] P. H. Chavanis, “Phase Transitions in Self-Gravitating Systems,” *International Journal of Modern Physics B*, vol. 20, pp. 3113–3198, 2006.
- [4] Ensemble inequivalence may arise in other systems with (non-gravitational) long range interactions as well, see A. Campa, T. Dauxois, and S. Ruffo, “Statistical mechanics and dynamics of solvable models with long-range interactions,” *Physics Reports*, vol. 480, pp. 57–159, Sept. 2009.
- [5] W. Thirring, “Systems with negative specific heat,” *Zeitschrift fur Physik*, vol. 235, pp. 339–352, Aug. 1970.
- [6] N. Bilić and R. D. Viollier, “Gravitational phase transition of fermionic matter in a general-relativistic framework,” *European Physical Journal C*, vol. 11, pp. 173–180, Nov. 1999.
- [7] P.-H. Chavanis, M. Lemou, and F. Méhats, “Models of dark matter halos based on statistical mechanics: The fermionic King model,” *Physical Review D*, vol. 92, p. 123527, Dec. 2015.
- [8] See P.-H. Chavanis and G. Alberti, “Gravitational phase transitions and instabilities of self-gravitating fermions in general relativity,” *arXiv e-prints*, Aug. 2019., and references therein.
- [9] J. G. Gao, M. Merafina, and R. Ruffini, “The semidegenerate configurations of a selfgravitating system of fermions,” *Astronomy and astrophysics*, vol. 235, pp. 1–7, Aug. 1990.
- [10] For this kind of two-parametric equation of state, this was demonstrated for the first time in C. R. Argüelles and R. Ruffini, “Are the most super-massive dark compact objects harbored at the center of dark matter halos?,” *International Journal of Modern Physics D*, vol. 23, p. 1442020, Oct. 2014.
- [11] R. Ruffini, C. R. Argüelles, and J. A. Rueda, “On the core-halo distribution of dark matter in galaxies,” *Monthly Notices of the Royal Astronomical Society*, vol. 451, pp. 622–628, July 2015.
- [12] I. Siutsou, C. R. Argüelles, and R. Ruffini, “Dark matter massive fermions and Einasto profiles in galactic haloes,” *Astronomy Reports*, vol. 59, pp. 656–666, July 2015.
- [13] L. G. Gómez, C. R. Argüelles, V. Perlick, J. A. Rueda, and R. Ruffini, “Strong lensing by fermionic dark matter in galaxies,” *Physical Review D*, vol. 94, p. 123004, Dec. 2016.
- [14] C. R. Argüelles, N. E. Mavromatos, J. A. Rueda, and R. Ruffini, “The role of self-interacting right-handed neutrinos in galactic structure,” *Journal of Cosmology and Astroparticle Physics*, vol. 4, p. 038, Apr. 2016.
- [15] C. R. Argüelles, A. Krut, J. A. Rueda, and R. Ruffini, “Novel constraints on fermionic dark matter from galactic observables I: The Milky Way,” *Physics of the Dark Universe*, vol. 21, p. 82, Sept. 2018.
- [16] C. R. Argüelles, A. Krut, J. A. Rueda, and R. Ruffini, “Novel constraints on fermionic dark

matter from galactic observables II: Galaxy scaling relations,” *Physics of the Dark Universe*, vol. 24, p. 100278, Mar. 2019.

- [17] C. R. Argüelles, A. Krut, J. A. Rueda, and R. Ruffini, “Can fermionic dark matter mimic supermassive black holes?,” *arXiv e-prints*, May 2019.
- [18] C. R. Argüelles and N. E. Grandi, “Fermionic halos at finite temperature in AdS/CFT,” *Journal of High Energy Physics*, vol. 5, p. 118, May 2018.
- [19] J. de Boer, K. Papadodimas, and E. Verlinde, “Holographic Neutron Stars,” *Journal of High Energy Physics*, vol. 2010, p. 020, oct 2010.
- [20] X. Arsiwalla, J. de Boer, K. Papadodimas, and E. Verlinde, “Degenerate Stars and Gravitational Collapse in AdS/CFT,” *Journal of High Energy Physics*, vol. 2011, p. 144, Jan 2011.
- [21] J. Katz, “On the number of unstable modes of an equilibrium,” *Monthly Notices of the Royal Astronomical Society*, vol. 183, pp. 765–770, June 1978.
- [22] G. Alberti, and P.-H. Chavanis, “Caloric curves of self-gravitating fermions in general relativity,” *arXiv e-prints 1808.01007*, aug 2018.